Analysis of a one mirror inclined three-mirror cavity photodetector for high-speed application

Yongqing Huang (黄永清), Cheng Huang (黄 成), Qi Wang (王 琦), Hui Huang (黄 辉), Xingyan Wang (王兴妍), and Xiaomin Ren (任晓敏)

School of Telecommunication Engineering, Beijing University of Posts & Telecommunications, Beijing 100876

Received August 30, 2004

There is a tradeoff between the quantum efficiency and the spectral response linewidth in resonant-cavity-enhanced (RCE) photodetectors. Recently a new type of photodetector structure has been proposed, which utilizes an inclined mirror in a three-mirror cavity. It decouples the quantum efficiency and the spectral response linewidth and has high response speed, high quantum efficiency, and narrow linewidth simultaneously. The analysis result indicates that the linewidth of 0.8 nm and quantum efficiency higher than 70% can be achieved on this device. For a 30×30 μm^2 device, the maximum bandwidth approaches 23 GHz.

OCIS codes: 230.0230, 230.5160, 250.0250.

With the development of telecommunication technology, wavelength-division-multiplexing (WDM) technology has become the focus of research and application for optical fiber communication systems. WDM systems need high performance and tunable photodetectors which have narrow linewidth and are capable of de-multiplexing. Especially, the de-multiplexing photodetectors are required to have linewidth equal or less than 0.8 nm, response speed greater than 10 Gb/s[1]. Resonant cavity enhanced (RCE) photodetector can effectively circumvent the tradeoff problem between quantum efficiency and bandwidth in traditional photodetectors, and as a result, high quantum efficiency and high bandwidth can be achieved simultaneously[2,3]. But the full-width at half-maximun (FWHM) of its spectral response is fairly wide and it is hard to get narrow spectral response linewidth less than 1.7 nm[4]. To decouple the spectral response linewidth and quantum efficiency of RCE photodetector, two new types of structures were proposed. One is parallel multi-cavity structure[5,6], in which narrow linewidth can be obtained only under exact design due to the coupling between the sub-cavities. The other type is one-mirror-inclined three-mirror-cavity (OMITC)[7,8] structure. The inclined mirror decouples the filtering cavity and the absorption cavity, so that the wavelength selectivity of the device only depends on the filtering cavity. An OMITC photodetector at central wavelength of 910 nm has been analyzed, designed, and fabricated in Refs. [7,8]. Though the absorption layer thickness is only 119 nm, the measured quantum efficiency is about 75%, and the FWHM of spectral response is 0.8 nm.

In this paper, an InP-based long wavelength one-mirror-inclined three-mirror cavity photodetector for high-speed application was analyzed. Numerical simulations demonstrate that the spectral response linewidth of the device is only 0.8 nm while the quantum efficiency is higher than 70%. For a 30×30 μm^2 area devices, the frequency response bandwidth is up to 23 GHz.

Figure 1(a) shows the schematic of OMITC photodetector. The bottom mirror M_1 and the middle mirror M_2 form the Fabry-Perot (F-P) filtering cavity. Above the filtering cavity is a PIN photodetector. The taper structure with inclined angle θ_0 is fabricated on epitaxial layer using dynamic mask etching. The inclined mirror M_3 is formed on the surface of the taper structure by depositing 6 periods of Si/SiO_2 distributed Bragg reflector (DBR). The absorption cavity consists of M_2, PIN photodetector, and M_3.

However the fabrication of InP-based long wavelength devices would meet some problems. For example, there is small difference in refractive index between the currently available materials, an inordinately large number of periods of quarter-wave dielectric layers and the stringent control of layer thickness are required to achieve high reflectivity of Bragg reflectors. To solve these problems we have proposed and fabricated InP-based long wavelength RCE photodetectors with InP/air-gap DBR[9]. To obtain InP-based high performance OMITC photodetectors, InP/air-gap DBR would also be introduced into the device to form the filtering cavity.

Figure 1(b) shows the analytical model of the device. When the device is back illuminated vertically, only the operating lightwave λ_0, which is determined by the filtering cavity, can transmit through the F-P cavity into the taper absorption cavity. With the specially chosen taper-angle θ_0, the filtering cavity functions as a highly

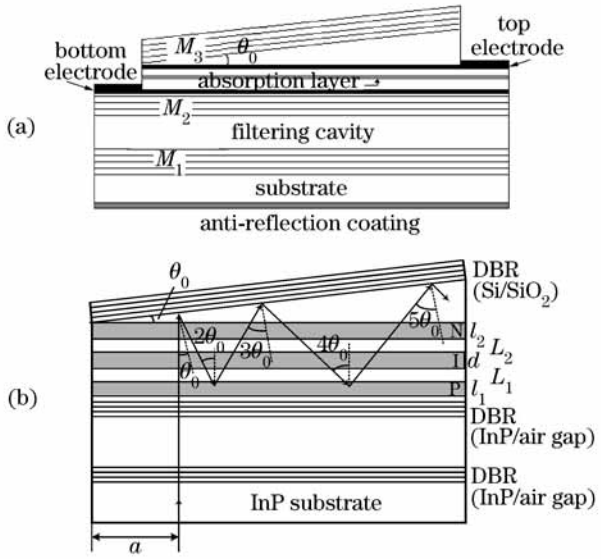

Fig. 1. The OMITC photodetector. (a) Schematic representation of the device; (b) analytical model.

reflective mirror for lightwave λ_0 reflected from the inclined mirror with different incident angles of $2\theta_0$, $4\theta_0$, $6\theta_0$, $8\theta_0$, $\cdots$. Therefore the operating lightwave can be well confined in the taper absorption cavity and experiences multiple reflections across the thin absorption layer in a zig-zag fashion. Thus, high quantum efficiency and wide bandwidth (owing to a thin absorption layer) can be achieved simultaneously. Moreover, owing to the nonresonant effect in the taper cavity, the wavelength selectivity can be solely determined by the filtering cavity for obtaining an ultra-narrow linewidth response, and wide range tuning can also be realized by using a micromechanical approach.

As shown in Fig. 1(b), when the operating lightwave experiences multiple reflection in the absorption cavity, the reflectivities of dielectric stacks DBR for TE and TM modes are different, and vary with the incident angle. While the incident angle increases, the thin dielectric film's optical length decreases, so the reflection band moves towards short wavelength direction. While λ_0 is out of the reflection band, the reflectivity for λ_0 drops drastically.

Lightwave transmitting through the F-P filtering cavity would be absorbed gradually while it experiences multiple reflections across the thin absorption layer. Based on Fig. 1(b), the quantum efficiency can be written as

$$\begin{aligned}\eta(\lambda,\theta_0) &= T(\lambda)\cdot A(\lambda,0) + T(\lambda)\cdot[1-A(\lambda,0)]\\ &\times R_{M_3}(\lambda,\theta_0)\cdot A(\lambda,2\theta_0) + T(\lambda)\cdot[1-A(\lambda,0)]\\ &\times R_{M_3}(\lambda,\theta_0)[1-A(\lambda,2\theta_0)]\cdot R_{\mathrm{F-P}}(\lambda,2\theta_0)\\ &\times A(\lambda,2\theta_0)+\cdots, \end{aligned} \tag{1}$$

where θ_0 is the inclined angle of M_3, $T(\lambda)$ is the transmission of filtering cavity for vertically incident lightwave, $A(\lambda,i\theta_0)=1-\exp[-\alpha(\lambda)\cdot d/\cos(i\theta_0)]$ ($i=0,\,2,\,4,\,\cdots$) is the absorptivity of the absorption layer, $R_{M_3}(\lambda,i\theta_0)$ is the reflectivity of the inclined mirror for incident angle $i\theta_0$ ($i=1,\,3,\,5,\,\cdots$), $R_{\mathrm{F-P}}(\lambda,i\theta_0)$ is the reflectivity of the F-P cavity for incident angle $i\theta_0$ ($i=2,\,4,\,6,\,\cdots$), d and $\alpha(\lambda)$ are the thickness and material absorption coefficient of the absorption layer ($In_{0.53}Ga_{0.47}As$).

When the reflection characteristics of the filtering cavity and the inclined mirror are known, the quantum efficiencies of TE and TM lightwave can be calculated using Eq. (1) respectively and then the total quantum efficiency by average. Figure 2 shows the quantum efficiency as a function of wavelength for $\theta_0=1^\circ$. The peak quantum efficiency is about 79% and the linewidth is 0.8 nm. Figure 3 shows the quantum efficiency as a function of the inclined angle, we can see that when $\theta_0=1^\circ$ the quantum efficiency reaches its maximum. This is because that the F-P filtering cavity has high reflectivity for lightwave with incident angle $\geq 2^\circ$, thus for $\theta_0=1^\circ$, the operating lightwave can experience the most times of reflections across the absorption layer to be absorbed.

It has been shown that the operating lightwave transmits through the absorption layer for a few times and for each time of absorption the PIN photodetector in the absorption cavity behaves just as a traditional PIN photodetector, so the response of the device may be the

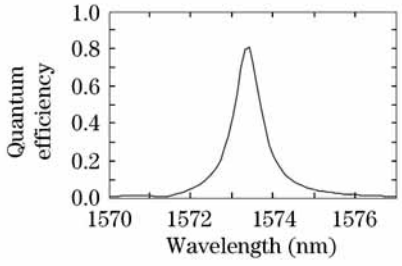

Fig. 2. Dependence of quantum efficiency on wavelength.

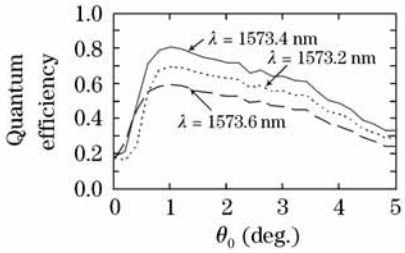

Fig. 3. Device's quantum efficiency as a function of the inclined angle θ_0.

summation of each effective absorption. Thus the frequency response and pulse response of the photodetector could be derived using the analytical method in Ref. [10].

When the device is back illuminated and the lightwave transmits through the absorption layer for the first time, the lightwave electric field component E_1 in the absorption layer is

$$E_1(x) = E_0 \mathrm{e}^{-\frac{1}{2}\alpha x}\mathrm{e}^{-j\beta x}, \tag{2}$$

where E_0 is the amplitude of lightwave electric field transmitting through the filtering cavity, α is absorption coefficient of the absorption layer, β is propagation constant of the absorption layer. The intensity distribution in absorption layer can be normalized from Eq. (2) as

$$f_1(x) = \mathrm{e}^{-\alpha x}. \tag{3}$$

Assuming impulse signal is detected, the electron and hole densities in the absorption layer after time t are

$$n_1(t) = \frac{1}{d+L_2}\Big[\int_{v_\mathrm{n}t}^{d} N_0 f_1(x-v_\mathrm{n}t)\mathrm{d}x\Big]\cdot u(\tau_\mathrm{n}-t),\quad t\geq 0, \tag{4}$$

$$p_1(t) = \frac{1}{d+L_1}\Big[\int_{0}^{d-v_\mathrm{p}t} N_0 f_1(x+v_\mathrm{p}t)\mathrm{d}x\Big]\cdot u(\tau_\mathrm{p}-t),\quad t\geq 0, \tag{5}$$

where u is unit step function, $\tau_\mathrm{n}=\frac{d}{v_\mathrm{n}}$, $\tau_\mathrm{p}=\frac{d}{v_\mathrm{p}}$ are the transit time of electrons and holes, v_p and v_n are saturated drift speeds of electrons and holes, N_0 is constant. The current densities caused by electrons and holes are

$$J_{\mathrm{n}1}(t) = qn_1\left(t-\frac{L_2}{v_\mathrm{n}}\right)v_\mathrm{n}u\left(t-\frac{L_2}{v_\mathrm{n}}\right),\quad t\geq 0, \tag{6}$$

$$J_{\mathrm{p}1}(t) = qp_1\left(t-\frac{L_1}{v_\mathrm{p}}\right)v_\mathrm{p}u\left(t-\frac{L_1}{v_\mathrm{p}}\right),\quad t\geq 0, \tag{7}$$

where L_1 is the thickness of spacing layer on the P side and L_2 on the N side. The time delay caused by the spacing layers is involved in Eqs. (6) and (7) as $\frac{L_2}{v_n}$ for electrons and $\frac{L_1}{v_p}$ for holes.

For the lightwave transmitting through the absorption layer for the mth (m is even and $m \geq 2$) time, the lightwave electric field component in the absorption layer is

$$E_m(x) = E_0 \exp[-\frac{1}{2}\alpha d\left(1+\sum_{i=4}^{m}\frac{2}{\cos(i-2)\theta_0}\right)-\frac{1}{2}\alpha_{ex}g_m]$$
$$\times \exp[-j\beta d\left(1+\sum_{i=4}^{m}\frac{2}{\cos(i-2)\theta_0}\right)-j\beta_{ex}g_m]$$
$$\times (r_2 r_3)^{m-3} e^{-\frac{1}{2}\alpha\frac{x}{\cos m\theta_0}} r_3 e^{-j\beta\frac{x}{\cos m\theta_0}}, \quad (8)$$

$$g_m = \sum_{i=0}^{\frac{m-2}{2}}\left\{\frac{h_i}{\cos[(2i+2)\theta]}+\frac{h_i}{\cos(2i\theta)}\right\}$$
$$-(l_1+L_1+d)\left(1+\frac{1}{\cos m\theta}\right), \quad (9)$$

$$\begin{cases} h_i = [\frac{\tan(\theta)+\tan(\frac{\pi}{2}-2i\theta)}{\tan(\frac{\pi}{2}-2i\theta)-\tan(\theta)}]\cdot h_{i-1}, & i \geq 1 \\ h_0 = l_1+L_1+d+L_2+l_2+a\cdot\tan(\theta), & i=0 \end{cases}, \quad (10)$$

where β_{ex} is the propagation constant outside the absorption layer, a is the length from the incident spot to the edge of the device, l_2 is the thickness of N region, α_{ex} is the absorption coefficient outside the absorption layer, g_m is the optical length that the lightwave propagates before transmitting through the absorption layer for the mth time, r_3 is the reflectivity of the inclined mirror.

The normalized intensity distribution in the absorption layer $f_m(x)$ is

$$f_m(x) = \exp[-\alpha d\left(1+\sum_{i=4}^{m}\frac{2}{\cos(i-2)\theta_0}\right)-\alpha_{ex}g_m]$$
$$\times (r_2 r_3)^{2(m-3)} r_3^2 e^{-\alpha\frac{x}{\cos m\theta_0}}. \quad (11)$$

Electron and hole densities in the absorption layer are

$$n_{m0}(t) = \frac{1}{d+L_2}[\int_0^{d-v_n t} N_0 f_m(x+v_n t)dx]\cdot u(\tau_n - t),$$
$$t \geq 0. \quad (12)$$

$$p_{m0}(t) = \frac{1}{d+L_1}[\int_{v_p t}^{d} N_0 f_m(x-v_p t)dx]\cdot u(\tau_p - t),$$
$$t \geq 0. \quad (13)$$

Considering the time delay of the mth absorption $\tau_m = \frac{g_m}{c/n}$, the electron and hole densities are

$$n_m = n_{m0}(t-\tau_m)u(t-\tau_m), \quad (14)$$

$$p_m = p_{m0}(t-\tau_m)u(t-\tau_m). \quad (15)$$

The electron and hole current densities are

$$J_{nm}(t) = qn_m\left(t-\frac{L_2}{v_n}\right)v_n u\left(t-\frac{L_2}{v_n}\right), \quad t \geq 0, \quad (16)$$

$$J_{pm}(t) = qp_m\left(t-\frac{L_1}{v_p}\right)v_p u\left(t-\frac{L_1}{v_p}\right), \quad t \geq 0. \quad (17)$$

For the kth (k is odd and $k \geq 3$) time transmitting through the absorption layer, the normalized lightwave electric field component in the absorption layer is

$$E_k(x) = E_m(d)e^{-\frac{1}{2}\alpha\frac{x}{\cos(k-1)\theta_0}}e^{-\frac{1}{2}\alpha_{ex}g_k}r_3 e^{-j\beta_{ex}g_k}$$
$$\times e^{-j\beta\frac{x}{\cos(k-1)\theta_0}}, \quad m=k-1, \quad (18)$$

$$f_k(x) = f_m(d)e^{-\alpha\frac{x}{\cos(k-1)\theta_0}}e^{-\alpha_{ex}g_k}r_3^2, \quad (19)$$

$$g_k = \sum_{i=0}^{\frac{k-2}{2}-1}\left\{\frac{h_i}{\cos[(2i-2)\theta]}+\frac{h_i}{\cos(2i\theta)}\right\}$$
$$-(l_1+L_1+d)\left\{1-\frac{1}{\cos[(k-1)\theta]}\right\}. \quad (20)$$

The electron and hole current densities can be calculated. Thus the total current density of the impulse response is

$$J_{imp}(t) = J_{n1}(t)+J_{p1}(t)+\sum[J_{nm}(t)+J_{nk}(t)]$$
$$+\sum[J_{pm}(t)+J_{pk}(t)]. \quad (21)$$

Considering the serial resistance and junction capacitance, according to theories of signal and system[11], the impulse response is

$$J_{impRC}(t) = J_{imp}(t) * J_{RC}(t), \quad (22)$$

where $J_{RC}(t)$ is the impulse response of RC circuit,

$$J_{RC}(t) = \begin{cases} \frac{1}{RC}e^{-t/RC}u(t), & t \geq 0 \\ 0, & t<0 \end{cases}. \quad (23)$$

The impulse response of the photodetector considering the effect of RC circuit is

$$J_{impRC}(t) = \frac{1}{RC}\int_0^{\infty} J_{imp}(\tau)e^{-(t-\tau)/RC}u(t-\tau)d\tau. \quad (24)$$

The frequency response of the device is the Fourier transform of its impulse response,

$$H(\omega) = \int_0^{\infty} J_{impRC}(t)e^{-jwt}dt. \quad (25)$$

The normalized impulse response of the device is

$$F(\omega) = 20\lg\left|\frac{H(\omega)}{H(0)}\right| \quad (\text{dB}). \quad (26)$$

As for device structure shown in Fig. 1(b), the thicknesses of P, N, and absorption layer are l_1 = 450 nm, l_2 = 300 nm, d = 100 nm, the total thickness of spacing layers is $L_1 + L_2$ = 650 nm. $L_1 < L_2$ is a reasonable design due to different saturation drift velocities of electrons and holes. Assume that the serial resistance is 50 Ω, the device area is 50×50 μm^2, the inclined angle of M_3 is $\theta_0 = 1.5°$. Figure 4(a) shows the impulse response of the photodetector involved with the effect of RC. The FWHM is fairly wide. The rising edge is caused by the delay of each absorption and the falling edge is caused by the drift time of carriers in the absorption layer and the spacing layer and the effect of RC. Figure 4(b) shows the device's frequency response and the 3-dB frequency is 9.1 GHz. The fairly big device area results in big junction capacitance, which limits the bandwidth.

The frequency response of OMITC photodetectors with 30×30 μm^2 area is shown in Fig. 5. The bandwidth is wider than 20 GHz. L_1 is an important parameter that affects the bandwidth. For 30×30 μm^2 area the optimal value for L_1 is 260 nm, and then the bandwidth reaches 23.1 GHz. To obtain wider bandwidth, $\frac{L_1+d}{v_p} = \frac{L_2+d}{v_n}$ should be satisfied during the design and under such condition the optimized impulse response is shown in Fig. 6 with a 6-ps FWHM. Compared with Fig. 4(a), the trailing tail is much shorter. Figure 7 shows the frequency response for 10×10 μm^2 area devices. The maximum 3-dB bandwidth reaches 59 GHz. It shows clearly the effect of device area to the frequency response. To avoid the effect of junction capacitance, a unique pattern ohmic contact layer could be used[12]. Thus the bandwidth is hoped to be wider than 50 GHz while maintaining high coupling efficiency.

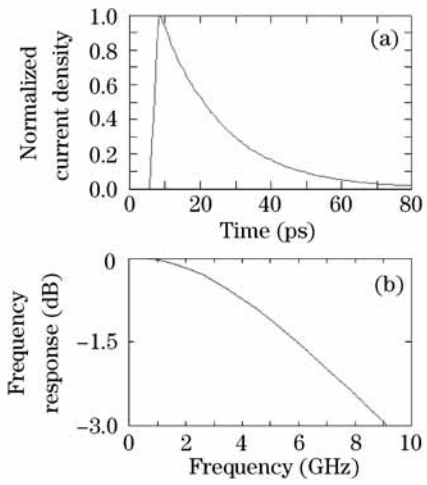

Fig. 4. The impulse response (a) and frequency response (b) of the device with L_1 = 200 nm, $s = 50 \times 50$ μm^2.

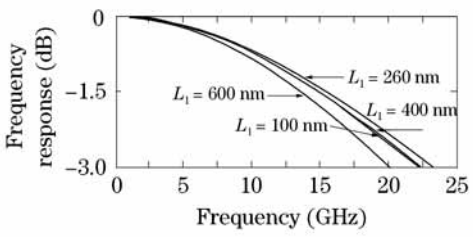

Fig. 5. The frequency response of the 30 × 30 μm^2 device.

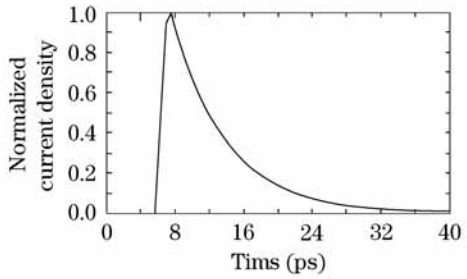

Fig. 6. The impulse response of the device with L_1 = 260 nm, $s = 30 \times 30$ μm^2.

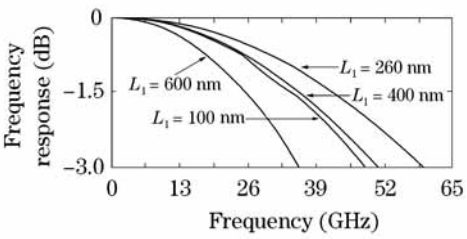

Fig. 7. The frequency response of the 10 × 10 μm^2 device.

This research was supported by the National High Technology R&D Program (No. 2003AA31g050, 2003AA312020), the Key Project of National Natural Science Foundation of China (No. 90201035), the Natural Science Foundation of Beijing (No. 4023013), the Project of Beijing Technology Program (No. H030430020330), and the Key Project of Science and Technology, Ministry of Education, P. R. China (No. 02028). Y. Huang's e-mail address is yqhuang@bupt.edu.cn.

References

1. S. Tsuda and V. L. da Silva, in *Proceedings of OFC2000* TuJ6-1 (2000).
2. K. Kishino, M. S. Ünlü, J.-I. Chyi, J. Reed, L. Arsenault, and H. Morkoc, IEEE J. Quantum Electron. **27,** 2025 (1991).
3. M. S. Ünlü and S. Strite, J. Appl. Phys. **78,** 607 (1995).
4. T. Knödl, H. K. H. Choy, J. L. Pan, R. King, R. Jäger, G. Lullo, J. F. Ahadian, R. J. Ram, C. G. Fonstad, Jr., and K. J. Ebeling, IEEE Photon. Technol. Lett. **11,** 1289 (1999).
5. X. Ren and J. C. Campbell, IEEE J. Quantum Electron. **32,** 1903 (1996).
6. K. Liu, Y. Huang, and X. Ren, Appl. Opt. **39,** 423620 (2000).
7. H. Huang, R. Zhang, Q. Wang, Y. Zhong, X. Wang, L. Lei, Y. Xia, L. Liu, Y. Huang, and X. Ren, in *Proceedings of OFC2002* ThGG73 (2002).
8. H. Huang, R. Zhang, Q. Wang, Y. Huang, and X. Ren, Chin. J. Lasers B **11,** 440 (2002).
9. Y. Q. Huang, H. Huang, Q. Wang, X. Y. Wang, Z. Zhou, and X. M. Ren, Semiconductor Optoelectronics (in Chinese) **24,** 230 (2003).
10. H.-H. Tung and C.-P. Lee, IEEE J. Quantum Electron. **33,** 753 (1997).
11. J. L. Zheng, W. L. Yang, and Q. H. Ying, *Signals and Systems* (in Chinese) (Higher Education Press, Beijing, 1981).
12. X. M. Ren, H. Huang, Y. Q. Huang, and Q. Wang, *High speed and high sensitivity resonant cavity enhanced (RCE) photodetector* China Practicality and New Type Patent ZL 01 2 75368.8. (June 2002).